Nature Climate Change - https://doi.org/10.1038/s41558-023-01757-7

Asymmetric influence of forest cover gain and loss on land surface temperature

Yongxian Su[1,2], Chaoqun Zhang[1,2], Philippe Ciais[3], Zhenzhong Zeng[4], Alessandro Cescatti[5], Jiali Shang[6], Jing Ming Chen[7], Jane Liu[7], Ying-Ping Wang[8], Wenping Yuan[1], Shushi Peng[9], Xuhui Lee[10], Zaichun Zhu[9], Lei Fan[11], Xiaoping Liu[1], Liyang Liu[1,2,3], Raffaele Lafortezza[12,13], Yan Li[14], Jiashun Ren[1,2], Xueqin Yang[1,2], Xiuzhi Chen[1]

1 Guangdong Province Data Center of Terrestrial and Marine Ecosystems Carbon Cycle, Guangdong Province Key Laboratory for Climate Change and Natural Disaster Studies, School of Atmospheric Sciences, School of Ecology, School of Geography and Planning, Sun Yat-sen University, Guangzhou, China;

2. Guangdong Provincial Key Laboratory of Remote Sensing and Geographical Information System, Guangdong Open Laboratory of Geospatial Information Technology and Application, Guangzhou Institute of Geography, Guangdong Academy of Sciences, Guangzhou, China;

3. Laboratoire des Sciences du Climat et de l'Environnement, IPSL, CEA-CNRS-UVSQ, Université Paris-Saclay, Gif sur Yvette, France;

4. School of Environmental Science and Engineering, Southern University of Science and Technology, Shenzhen, China;

5. European Commission, Joint Research Centre, Ispra, Italy;

6. Ottawa Research and Development Centre, Agriculture and Agri-Food Canada, Ottawa, Ontario, Canada;

7. Department of Geography and Planning, University of Toronto, Toronto, M5S 3G3, Ontario, Canada;

8. CSIRO Environment, Aspendale, Victoria, Australia;

9. College of Urban and Environmental Sciences, Peking University, Beijing, China;

10. School of the Environment, Yale University, New Haven, CT, USA;

11. School of Geographical Sciences, Southwest University, Chongqing, China;

12. Department of Soil, Plant and Food Sciences, University of Bari "Aldo Moro", Via Amendola 165/A, 70126 Bari, Italy;

13. Beijing Forestry University, Beijing 100083, China;

14. State Key Laboratory of Earth Surface Processes and Resources Ecology, Beijing

Normal University, Beijing, 100875, China

Corresponding author: X. Chen (chenxzh73@mail.sysu.edu.cn)

Abstract

In recent decades, forests globally experienced tree cover gains and losses, often in a fine-scale process. While the biogeochemical implications of such changes on carbon storage are recognized, the direct biophysical effects of fine-scale tree cover gains and losses on land surface temperature are less well understood. Here we show how land surface temperature at 0.05° resolution grid cell responds to sub-grid gross tree cover changes. We find that in tropical forests, the biophysical cooling induced by enhanced evapotranspiration per unit area of tree cover gain is greater in magnitude than the warming from tree cover loss. The goal of no biophysical warming effects from tree cover changes could be achieved by regaining > 75% of previously lost tree cover areas. In temperate forests, this minimum fraction increases to 83%. In boreal forests, however, the biophysical cooling from per unit area of tree cover loss due to increasing albedo outweighs the warming from tree cover gain, and a tree cover loss should be greater than 66% of tree cover gain to achieve the goal of zero local biophysical warming. Neglecting this asymmetric temperature effect of fine-scale tree cover gain and loss ignores the fact that biophysical feedbacks continue to cause surface temperature changes even under net-zero tree cover changes. Thus, it is necessary to account for gross, rather than net, tree cover changes when quantifying the biophysical effects of forests.

Introduction

Forests store 45% of terrestrial carbon and remove from the atmosphere a large amount of carbon dioxide released by human activities to mitigate global warming[1,2]. This process leads to a global biogeochemical cooling effect by reducing the radiative forcing of carbon dioxide[3]. In addition, forests influence the land-atmosphere exchange of energy and water[4-9] and exert direct biophysical effects on global surface temperatures through radiative processes (albedo)[10] and nonradiative processes (latent and sensible heat fluxes)[11-13]. Forests also have indirect biophysical feedbacks on climate through atmospheric coupling, e.g. atmospheric circulation, cloud formation, and precipitation[4,14]. During the twenty-first century, forests have experienced dramatic changes (i.e., land cover conversions and tree cover changes in forests remaining forests)[15,16], affecting their biogeochemical trace gases exchange[11] and biophysical processes[5,9,17-19].

At the global scale, studies on biogeochemical[11,20,21] and biophysical temperature effects[22-24] of forests have mainly focused on land cover change such as afforestation and deforestation. The biogeochemical effect is quantified by calculating the carbon difference between forest and neighboring nonforest grid cells, which is then converted to a global temperature change. The biophysical effect is quantified by interpreting spatial differences in temperature, mainly satellite-based land surface temperature (*LST*)[21]. These approaches rely on the space-for-time analogies where spatial gradients in carbon storage or *LST* between forest and neighboring nonforest are used as proxies for estimating temporal changes of biogeochemical or biophysical effects[7,25].

However, significant fine-scale tree cover changes (gains and losses) have occurred in forests remaining forests worldwide[15], mainly due to natural disturbance, forest management, and other changes in canopy density[26,27]. Although these tree cover gains and losses in established forests are not a land cover conversion, they can still impact the global carbon balance[28,29]. High-resolution satellite carbon data have been used to assess such biogeochemical implications induced by fine-scale tree cover changes based on the space-for-time analogy method[11,20,21]. Nevertheless, challenges remain for quantifying the direct biophysical *LST* effects induced by fine-scale tree cover changes[5,18,30-36]. This is an important research question because *LST* is monitored globally from satellites with frequent revisits only at a kilometric-scale spatial resolution whereas changes in tree cover can be assessed at a finer scale of 30 meters. Alkama and Cescatti developed a methodology to estimate *LST* change caused by direct biophysical effects of 30-m resolution net tree cover changes using satellite-based time-series data[5], known as the time-series analysis method[37].This approach was, however, only applied to net changes in tree cover[5,30] and did not investigate the distinct biophysical effects caused by gross tree cover gain and loss within a *LST* grid cell.

To address this knowledge gap, we focused on forest areas that had undergone fine-scale gross tree cover changes while not changing land cover (hereinafter referred to as sub-grid tree cover gain and loss with respect to the coarser scale *LST* observations). We aimed to quantify the differences of direct biophysical *LST* effects induced by sub-grid tree cover gains versus losses from 2000 to 2012. To do so, we first selected 0.05° forest grid cells that were classified as "forestlands" on the Moderate Resolution Imaging Spectroradiometer (MODIS) land cover product[38,39]. We then classified a forest grid cell as "disturbed" if it experienced more than 2% of sub-grid change in tree cover gain (f_{gain}>0.02) or loss (f_{loss}>0.02) based on 30-m resolution tree cover maps from Global Forest Watch (*GFW*)[15] during 2000-2012. Correspondingly, we classified a forest grid cell as "undisturbed" if it experienced less than 2% of gross tree cover change (i.e., f_{gain}≤0.02 and f_{loss}≤0.02) and showed a stable Normalized Difference Vegetation Index ($\Delta NDVI$=0±0.02). We used the 0.05° resolution MOD11C3 v061 LST product[38] to calculate the LST anomaly between 2000 and 2012 for each forest grid cell. Finally, the *LST* anomaly of neighboring undisturbed grid cells caused by climate variability alone (ΔLST_{cv}) was removed from the signals of the disturbed grid cells to extract the direct biophysical effects on *LST* caused by sub-grid tree cover changes (ΔLST_{fc}), following the methodology of Alkama and Cescatti[5] adapted with more stringent criteria (**see Methods** for details). Only those disturbed grid cells with more than 5 reference undisturbed grid cells within a 50-km distance[5] were included in the analysis.

Main

Global patterns of ΔLST_{fc} induced by tree cover changes in forests

Globally, 34.7% of all the 0.05° forest grid cells were classified as disturbed forests, with 10.3% being located in tropical regions, 6.8% in temperate regions, and 17.6% in boreal regions (**Fig. 1a**). Approximately 57.4% of these disturbed forest grid cells, mainly in tropical (20°N-20°S) and boreal regions (Canada and eastern Russia), experienced a net tree cover loss defined by $f_{net}= f_{gain}-f_{loss}<-0.02$. Conversely, only 19.1% of the disturbed forests experienced net gains ($f_{net}>0.02$), with these forests located mostly in Europe, western Russia, and southern Brazil. The remaining 23.5% of the disturbed forests showed no significant net changes in tree cover (f_{net} =0±0.02).

We found that some disturbed forests that experienced a net tree cover loss were still associated with a biophysical cooling effect (**Fig. 1a, b**), especially in tropical and temperate forest grid cells that experienced large fractions of gross tree cover gain, such as in the eastern United States (f_{net}=-0.01±0.004, f_{gain}=0.13±0.003, daily mean ΔLST_{fc} =-0.05±0.002°C), eastern Congo (f_{net}=-0.05±0.003, f_{gain}=0.06±0.002, daily mean ΔLST_{fc} =-0.03±0.009°C), and subtropical southern China (f_{net}=-0.02±0.003, f_{gain}=0.06±0.003, daily mean ΔLST_{fc} =-0.04±0.006°C) (**Fig. 1e, f**). This result is different from previous findings where deforestation was systematically associated with significant warming[5,9,22,23]. This phenomenon occurred because for the same value of f_{net}, the sign and magnitude of ΔLST_{fc} depended significantly on the absolute values of f_{gain} (**Fig. S1**). Therefore, we quantified the sensitivity of ΔLST_{fc} to a unit of gross tree cover gain (S_{gain}) and loss (S_{loss}) (see **Methods**). For the global average, S_{gain} (-0.81±0.024°C) (**Fig. 1c**) was greater in absolute value than S_{loss} (0.66±0.021°C) (**Fig. 1d**). The difference in magnitude between S_{gain} and S_{loss} was typically negative in temperate and tropical zones, for instance, in the eastern United States (S_{gain}=-0.76±0.037°C; S_{loss}=0.59±0.027°C), eastern Congo (S_{gain}=-0.80±0.091°C; S_{loss}=0.53±0.095°C) and subtropical southern China (S_{gain}=-0.98±0.098°C; S_{loss} =0.70±0.102°C) (**Fig. 1c, d, g, h**).

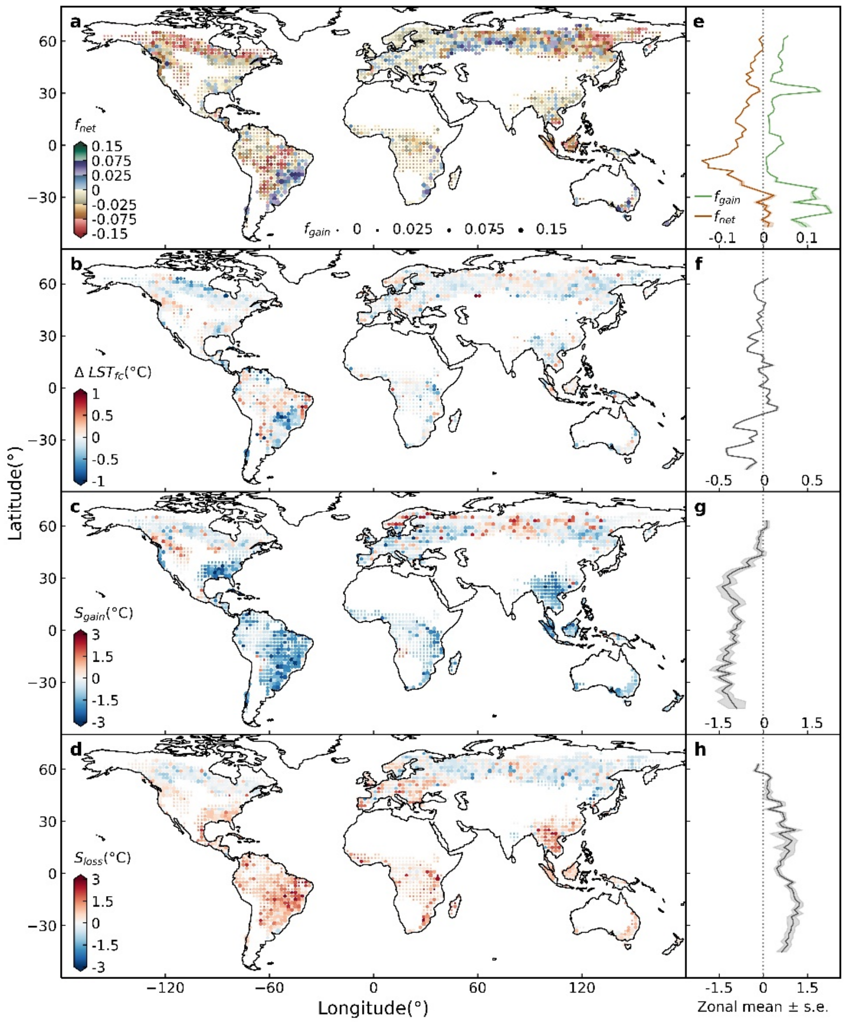

Fig. 1 Global patterns of tree cover changes in disturbed forests during the 2000-2012 time period and their direct biophysical effects on daily mean land surface temperature (ΔLST_{fc}). (**a**) Net fractional change in tree cover (*f_{net}*) over 0.05° disturbed grid cells that remained forests from 2000 to 2012, (**b**) daily mean ΔLST_{fc} induced by tree cover gains and losses in disturbed forests, (**c**) sensitivity (S_{gain}) of the daily mean ΔLST_{fc} to gross tree cover gain (f_{gain}), and (**d**) sensitivity (S_{loss}) of the daily mean ΔLST_{fc} to gross tree cover loss (f_{loss}). The dots in panels **a-d** are spaced at 2° for both latitude and longitude. The right-hand panels **e-h** show zonal mean values of changes in tree cover fractions, ΔLST_{fc}, S_{gain} and S_{loss} averaged into 2° latitude bins, respectively. The shading represents one standard error.

Asymmetric influence of tree cover gain and loss on ΔLST_{fc}

The spatial variations in ΔLST_{fc} and its distinct sensitivity to f_{gain} and f_{loss} shown in **Fig. 1** raise two questions: (1) What are the values of ΔLST_{fc} in disturbed forests with net-zero change in tree cover (f_{gain}=f_{loss})? and, (2) what are the values of f_{gain} versus f_{loss} in disturbed forests that result in net-zero change in LST (ΔLST_{fc}=0±0.02°C), that is, the LST anomaly induced by the direct biophysical effect of gross tree cover loss is offset by that induced by gross tree cover gain (hereinafter referred to as LST neutrality)? Answering the first question involves quantifying how disturbed forests with a stable tree cover fraction composed of gross tree cover gain and loss in equal magnitude impact local LST. Answering to the second question provides a benchmark of f_{gain} versus f_{loss} against which sub-grid tree cover changes in forest grid cells could be managed to achieve a net direct biophysical LST cooling.

The plots in **Fig. 2** show the variations in ΔLST_{fc} in disturbed forest grid cells with all combinations of f_{gain} and f_{loss}. In tropical and temperate forests, daytime ΔLST_{fc} was more negative (cooling) with increasing f_{gain} and more positive (warming) with increasing f_{loss} (**Fig. 2a, b**). Nighttime ΔLST_{fc} generally responded in the opposite manner (**Fig. 2d, e**) but with a smaller absolute value than daytime ΔLST_{fc}. Consequently, in tropical and temperate forests, the daily mean ΔLST_{fc} (**Fig. 2g, h**) was dominated by daytime ΔLST_{fc} signal. In boreal forests, however, the daily mean ΔLST_{fc} (**Fig. 2i**) largely depended on nighttime ΔLST_{fc} (**Fig. 2f**) which had a greater magnitude than daytime ΔLST_{fc} (**Fig. 2c**). The daily mean ΔLST_{fc} in this biome was more positive (warming) with increasing f_{gain} and more negative (cooling) with increasing f_{loss} (**Fig. 2i**).

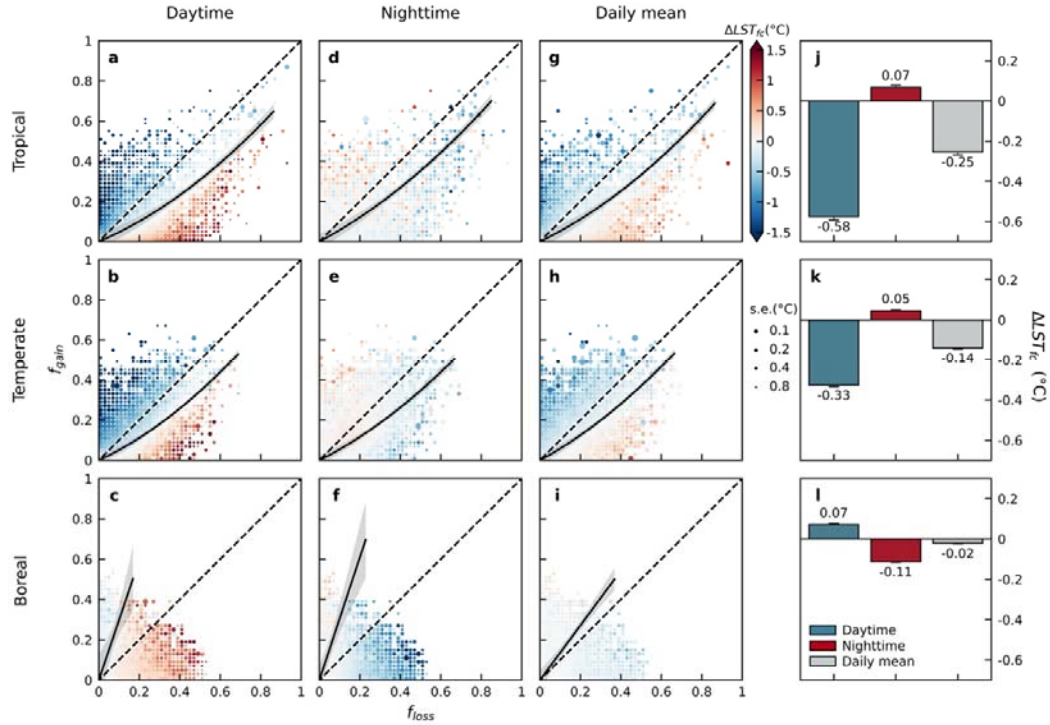

Fig. 2 Changes in daytime (a-c), nighttime (d-f), and daily mean (g-i) land surface temperature (ΔLST_{fc}) induced by direct biophysical effects of tree cover changes with various fractions of tree cover gain (f_{gain}) and loss (f_{loss}) in different climate zones from 2000 to 2012. Plots **j-l** show the average ΔLST_{fc} in disturbed forest grid cells with equivalent f_{gain} and f_{loss} (i.e., f_{net}=0±0.02). Each cell in the bubble matrix shows the average ΔLST_{fc} observed for a given combination of f_{gain} and f_{loss} within 0.05° grid cells from 2000 to 2012 reported on the X- and Y-axes in the 0.02 bin, respectively. Red denotes a warming effect (ΔLST_{fc}>0.02°C), blue denotes cooling (ΔLST_{fc}<-0.02°C), and grey represents *LST* neutrality (ΔLST_{fc}=0.0±0.02°C) induced by direct biophysical effects of tree cover gains and losses. The size of the dot indicates the degree of one standard error. The black dashed 1:1 lines represent equal fractions of tree cover gain and loss (i.e., f_{gain}=f_{loss}). The black solid curves, named the *LST*-neutral curves, are fitted by quadratic models based on the scatter between f_{gain} and f_{loss} for grid cells with ΔLST_{fc} =0.0±0.02°C (see **Methods**), thereby separating the biophysical cooling and warming effects on *LST*. The shading represents the 95% confidence interval assessed by bootstrapping across each grid cell (n=500). The significance (p value) of all fitted curves is less than 0.001. Error bars are given as two

standard errors.

Fig. 2 shows that warming and cooling on *LST* induced by direct biophysical effects of tree cover changes were not symmetrically distributed along the 1:1 diagonal line defining f_{gain}=f_{loss}. The relationship between f_{gain} and f_{loss} for disturbed forest grid cells corresponding to *LST* neutrality (ΔLST_{fc}=0.0±0.02°C) can be approximated using a quadratic function, i.e., f_{gain}= $q(f_{loss})$ (see **Methods**), which is shown by the black solid curves in **Fig. 2** (hereinafter referred to as the *LST*-neutral curves). In tropical and temperate forests, this quadratic function laid below the 1:1 diagonal line, indicating a negative asymmetry of f_{gain} on biophysical *LST* neutrality (**Fig. 2a, b, d, e, g, h**). Consequently, the grid cells with f_{gain}=f_{loss} were associated with a significant daytime cooling effect (tropical: -0.58±0.009°C, temperate: -0.33±0.004°C) and a small nighttime warming effect (tropical: 0.07±0.005°C, temperate: 0.05±0.002°C), leading to an overall cooling effect of the daily mean *LST* (tropical: -0.25±0.007°C, temperate: -0.14±0.003°C) (**Fig. 2j, k**). Conversely, in boreal forests, the q function was above the 1:1 line, implying a positive asymmetry of f_{gain} on biophysical *LST* neutrality (**Fig. 2c, f, i**). Grid cells with f_{gain}=f_{loss} showed a warming effect on daytime *LST* (0.07±0.002°C) and a stronger cooling effect on nighttime *LST* (-0.11±0.002°C), resulting in a slight cooling effect on the daily mean *LST* (-0.02±0.002°C) (**Fig. 2j**). Additionally, these asymmetric responses of ΔLST_{fc} with respect to f_{gain} versus f_{loss} were still robust to the choice of another time period (2003-2012, 2006-2012 and 2009-2012), for larger *LST* grid-cell sizes (0.1° instead of 0.05°) and under different thresholds of final tree cover for estimating f_{gain} in disturbed forests (**Figs. S2-6**) (see **Methods** for details).

To quantify the asymmetry influences of f_{gain} versus f_{loss} on *LST*, we calculated the ratio of f_{gain} to f_{loss}, hereinafter referred to as ρ, in disturbed grid cells with biophysical *LST* neutrality (daily mean ΔLST_{fc}=0.0±0.02°C). Over the globe, ρ showed a distinctive latitudinal gradient (**Fig. 3** and **Fig. S7**). In tropical forests, ρ had the smallest values, i.e., below 1.0 (average ρ=0.75±0.025) (**Fig. 3a**), suggesting that lower gains in tree cover than losses can achieve *LST* neutrality for this biome. Within tropical forest regions, ρ was smaller in tropical Africa than in tropical South America and tropical Asia. In temperate forests, the value of ρ was larger than that of tropical forests (average ρ=0.83±0.051) (**Fig. 3a**) and increased significantly with latitude (**Fig. 3b**). In boreal forests, ρ mostly varied between 1.0 and 2.0 (average ρ=1.51±0.224) and was the highest in Siberia (**Fig. 3a**). In this biome, if only the direct biophysical effect was considered, the ratio of f_{gain} to f_{loss} must be smaller than ρ to achieve a negative *LST* anomaly.

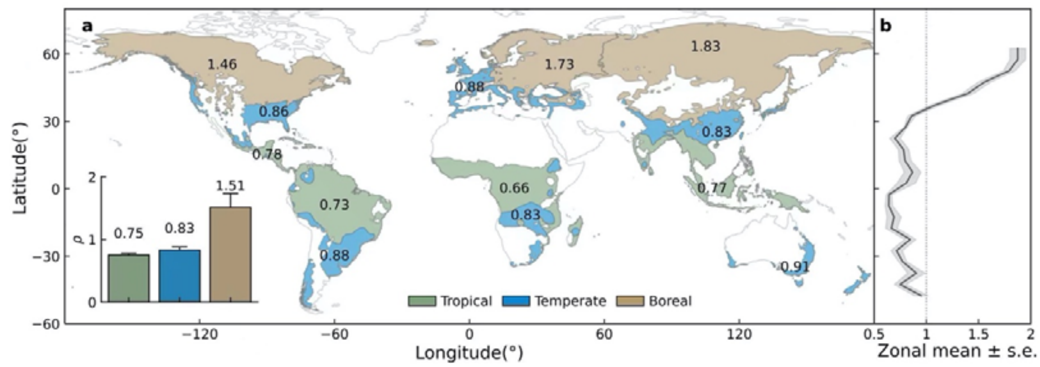

Fig. 3 Ratio of f_{gain} to f_{loss} (ρ) in disturbed forest grid cells with land surface temperature neutrality (daily mean ΔLST_{fc}=0.0±0.02°C) induced by direct biophysical effects of tree cover gains and losses in different climate regions (a) and at different latitudes (b) around the globe. The inset histograms in plot **a** represent mean ρ values in the tropical, temperate and boreal climate zones, respectively. The light green, light blue and light brown colours on the global map indicate the tropical, temperate and boreal climate regions, respectively. The floating numbers on the map represent the average ρ values for the corresponding regions. Error bars are given as one standard error. The curve in plot **b** indicates the median values of ρ in 5° latitude bins. The shading represents one standard error.

Mechanisms of the asymmetrical impact on ΔLST_{fc}

The asymmetric responses of ΔLST_{fc} with respect to f_{gain} and f_{loss} can be explained by the asymmetric influences of tree cover gain versus loss on the surface energy balance[7,40-44] (**Fig. 4a-l** and **Fig. S8**), which were diagnosed using satellite observations of albedo, shortwave downwelling radiation (SW) and latent heat (LE) turbulent fluxes (see **Methods** for details).

In the tropical and temperate forests, the neutral curves for changes in the surface energy fluxes were all below the 1:1 diagonal line in the [f_{gain}, f_{loss}] spaces (**Fig. 4a, b, d, e, g, h, j, k**). Disturbed tropical forests with f_{gain}=f_{loss} showed lower values of reflected SW (albedo multiplied by incoming SW) (ΔSW=-0.9±0.2W/m^2) (**Fig. 4m**), higher values of LE (ΔLE=5.1±0.4W/m^2) (**Fig. 4n**), and small increases in sensible heat and ground heat fluxes ($\Delta(H+G)$=0.2±0.1W/m^2) (**Fig. 4o**) compared with undisturbed forests. Overall, these processes caused a significant net decrease in surface energy budget (ΔLW=-4.4±0.2W/m^2) (**Fig. 4p**), which explained the cooling signal shown in **Fig. 2**. In temperate forests, the grid cells with f_{gain}=f_{loss} showed a moderate cooling effect, indicated by a moderate reduction in SW reflection (ΔSW=-0.5±0.1W/m^2) (**Fig. 4m**), a moderate increase in LE (ΔLE=2.0±0.2W/m^2) and H and G fluxes ($\Delta(H+G)$=0.4±0.1W/m^2) (**Fig. 4o**). In these two biomes, the stronger increase in evapotranspiration (ET) associated with tree cover gain compared to the decrease from tree cover loss was the main cause of the negative asymmetry of f_{gain} on ΔLST_{fc} in the disturbed forests, where tree cover losses were mainly induced by commodity-driven deforestation, shifting agriculture, and forestry[40] (inset histograms in **Fig. 4a, b, d, e, g, h, j, k; Figs. S9-14**). This is because the young trees associated with tree cover gain are usually shorter and have higher leaf water potentials and a consequent larger ET than the previous tree cover[45-49]. In contrast, the changes in reflected SW induced by albedo differences were negligible between newly grown young trees and previously lost older trees[42,43]. These processes eventually led to a negative asymmetric influence of tree cover gain versus loss on ΔLST_{fc} (**Fig. 2**). By matching GFW data[15] with planting years from a new global map of plantations[50] (see **Methods** for details), we show that the LST-neutral curves for plantations older than 6 years were slightly more distant from the 1:1 diagonal lines than those of younger plantations (**Fig. 5a, b**), indicating that tree age is one vital factor influencing the asymmetry of f_{gain} versus f_{loss} on ΔLST_{fc}. A space-for-time analysis over a longer period indicated that direct biophysical cooling of plantations on LST diminished as planted trees became older than approximately 28 years in tropical regions and 32 years in temperate regions (**Fig. 5c**). This result implies that influences of tree age on asymmetric patterns of ΔLST_{fc} may become weaker when trees exhibit lower growth rates[51] (see **Methods**).

In boreal forests, the situation is different. The neutral curves in the [f_{gain}, f_{loss}] spaces were above the 1:1 diagonal line for ΔSW and $\Delta(H+G)$ and below the 1:1 diagonal line for ΔLE (**Fig. 4c, f, i**). Disturbed grid cells in which f_{gain}=f_{loss} were associated with a large increase in reflected SW (ΔSW=1.8±0.3W/m^2) (**Fig. 4m**), a small increase in ET (ΔLE=0.5±0.2W/m^2) (**Fig. 4n**) and a strong decrease in H and G ($\Delta(H+G)$ =-1.3±0.2W/m^2) (**Fig. 4o**). These processes resulted in a minor decrease in the surface energy budget (ΔLW=-1.0±0.1W/m^2) (**Fig. 4l, p**) and thus a negligible biophysical cooling effect (**Fig. 2**). Therefore, the change in SW was the main cause for the asymmetric changes in the surface energy balance caused by tree cover gain versus loss whereas tree age-induced ET changes played a less important role. The stronger contribution of SW changes in boreal forests was mainly attributed to the lower forest albedo during snow-covered periods[6,52-54], typically 20% to 50% less than in snow-covered open areas. In addition, the dominant coniferous forests in boreal region[13] were typically darker (lower albedo)[6] than broadleaved trees prevailing elsewhere[55,56]. Forestry and wildfire were the two dominant causes of tree cover losses in disturbed boreal forests (inset histogram **in Fig. 4c, f, i, l; Figs. S9-14**). However, standing dead trees at recently burnt sites only partially masked winter snow cover and led to a weaker albedo increase than from timber harvest[7,18], which caused a strong increase in the reflected SW for forestry compared to wildfire (**Fig. 4c** and **Fig. S12**). Therefore, forestry-induced net changes in SW seem to be the main driver of the asymmetric response of ΔLST_{fc} in boreal forests where f_{gain}=f_{loss}. This finding is consistent with previous studies[5,24,42,57] that showed that albedo-induced net change in SW was the major cause of the change in direct biophysical effects on LST over boreal forests.

To assess the uncertainties of satellite-based retrievals of the surface energy balance, in addition to the MODIS ET dataset[58] used above, we tested two alternative datasets: the 0.05° resolution ET data products from Global Land Surface Satellite (GLASS)[59] and Penman-Monteith-Leuning (PML_v2) ET[60]. These two different ET

datasets (**Fig. S18**) showed marginally small differences compared with those derived from MODIS *ET* (**Fig. S8d-f**), confirming the robustness of the explanations for the observed asymmetry patterns of ΔLST_{fc}.

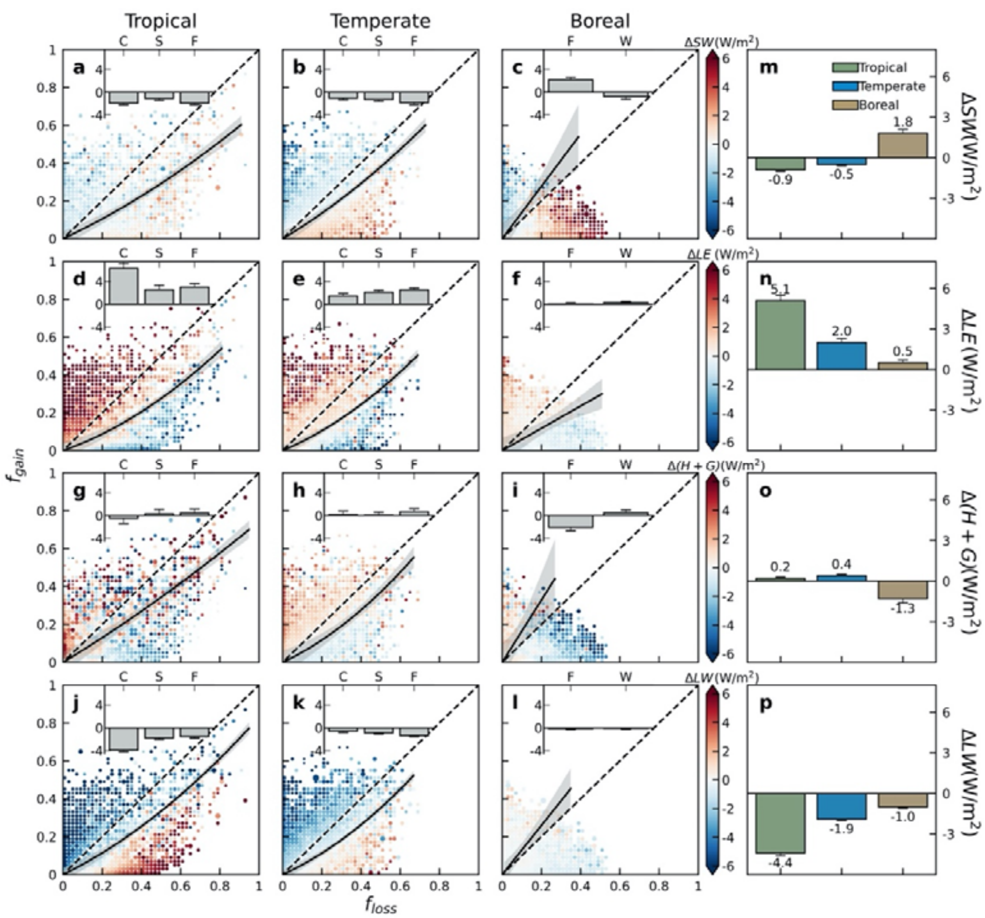

Fig. 4 Changes in surface energy balance components (reflected shortwave radiation from the surface [ΔSW, a-c], latent heat [ΔLE, d-f], sensible heat and ground heat fluxes [$\Delta(H+G)$, g-i], and emitted longwave radiation from the surface [ΔLW, j-l]) induced by tree cover changes with various fractions of tree cover gain (f_{gain}) and loss (f_{loss}) in different climate zones from 2000 to 2012. Δ stands for the difference between disturbed and undisturbed forests. Each cell in the bubble matrix shows the average value of each energy flux component for a given combination of f_{loss} and f_{gain} in 0.05° pixels on the X- and Y-axes in the 0.02 bin, respectively. Red indicates a positive value, blue indicates a negative value, and grey indicates a value of zero. The size of the dot indicates the degree of one standard error.

The black dashed 1:1 diagonal lines represent equal values of tree cover gain and loss (i.e., $f_{gain}= f_{loss}$). The neutral curves are fitted by quadratic models based on the scatters between f_{gain} and f_{loss}, similar to the *LST* neutral curves in **Fig. 2**. The shading represents the 95% confidence interval assessed by bootstrapping across each pixel (n=500). The significance (p value) of all fitted curves is less than 0.001. The average anomaly of each component in the surface energy balance induced by tree cover changes with equivalent f_{gain} and f_{loss} (i.e., f_{net}=0±0.02) is shown in plots **m-p**, while their further details for forest grid cells disturbed by different drivers are graphed as inset histograms in plots **a-l**. C, S, F and W denote commodity-driven deforestation, shifting agriculture, forestry and wildfire, respectively. Error bars are given as one standard error.

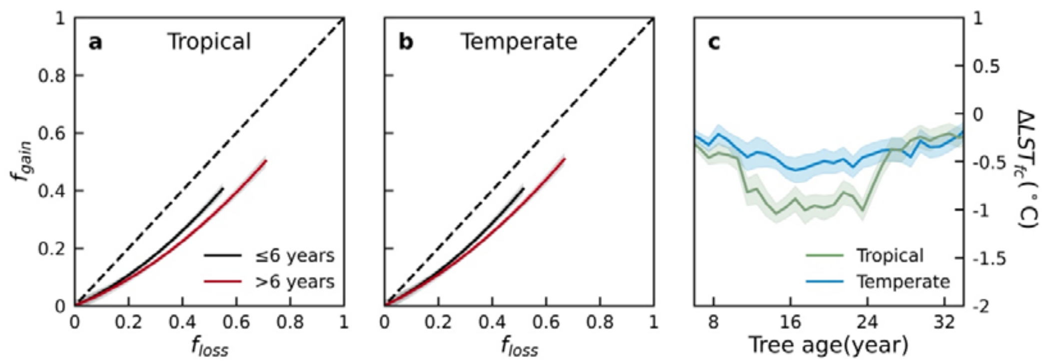

Fig. 5 Influences of tree age on the asymmetric pattern of ΔLST_{fc} induced by direct biophysical effects of tree cover gain and loss in tropical and temperate forests. (**a-b**) *LST*-neutral curves for disturbed forest grid cells with different planting ages (black: planting age≤6 years; red: 6 years<planting age≤12 years) in tropical (**a**) and temperate (**b**) zones. The *LST*-neutral curves are fitted by quadratic models (see **Figs. S15 and S16** for details). (**c**) Variations in the daily mean ΔLST_{fc} along with tree age (bin times: 1-year) in planted forests. Tree age influenced ΔLST_{fc} in planted forests with different tree covers (i.e., 50%< f_{gain}≤70% versus f_{gain}>70%), as shown in **Fig. S17**. The shading represents the 95% confidence interval, assessed by bootstrapping across each pixel (n=500). The significance (p value) of all fitted curves is less than 0.001.

Reliability of tree cover change data and potential impacts on the asymmetric patterns of $\Delta \boldsymbol{LST_{fc}}$

By comparing with the tree cover data recorded by the Food and Agriculture Organization of the United Nations (FAO), a standard reference for global-scale forest resource information produced at decadal intervals, previous studies indicated that significant uncertainties exist in some regions (such as Canada, China, Brazil) in the *GFW* tree cover data[61-63]. This is partially due to that *GFW* tree cover data could reflect tree cover changes caused by not only harvest activities but also natural disturbances in unmanaged forests which were not in the scope of field forest inventories[64]. To address this issue, here we used alternative tree cover maps from individual countries or regions including Canada[65], USA[66], eastern Europe[67], northern Europe[68], China[69] , and tropical moist forests[70] (**Table S2 and Fig. S19**), which were calibrated or validated using national forest cover statistics or field inventory data (**Fig. S20**) and were assumed to be more accurate than *GFW* tree cover data[71], as a means to provide an alternative data source for tree cover gain and loss[72].

Generally, the distributions of *LST*-neutral curves in the [f_{gain}, f_{loss}] spaces, based on the five regional tree cover datasets, were always on the same side of the 1:1 diagonal line as those generated by corresponding *GFW* tree cover data (**Figs. S21-26**), indicating the robustness of our findings on the asymmetric response of ΔLST_{fc} to f_{gain} versus f_{loss} at the global scale. In temperate forests, for example in the USA, both f_{gain} and f_{loss} agreed well with those from the National Land Cover Database (*NLCD*)[66] (**Fig. S21**), and the ρ difference ($\Delta\rho$) for the *LST*-neutral curves between *NLCD* and *GFW* tree cover data was approximately equal to zero. However, an underestimation of tree cover gains often occurred in regions with large afforestation programs such as China [22], the largest tree-planting country in the world. Thus, the negative asymmetry of f_{gain} on *LST* neutrality in China from *GFW* data was significantly weakened ($\Delta\rho$=0.07±0.019), but the *LST*-neutral curves from regional data were still below the 1:1 diagonal line (**Fig. S22**). In tropical moist forests, the lower performance of *GFW* tree cover data mainly stemmed from an overestimation of tree cover compared with an underestimation in dry tropical forests[73-75]. Our analyses showed that 68% of disturbed pixels in *GFW* tree cover data had a lower value of f_{loss}, ten percent smaller than the regional data from Joint Research Centre[70]. The negative asymmetry of f_{gain} on *LST* neutrality for this biome was to some extent underestimated in *GFW* tree cover data ($\Delta\rho$=-0.07±0.008) (**Fig. S23**).

The situations differ in the boreal forests of eastern Europe, northern Europe, and Canada. In eastern Europe, f_{gain} and f_{loss} of *GFW* tree cover data were almost equally underestimated compared with a more accurate regional data from the Global Land Analysis and Discovery Laboratory[67], and the asymmetry patterns of ΔLST_{fc} changed marginally ($\Delta\rho$=0.03±0.001) (**Fig. S24**). However, in countries such as Norway, Finland, and Sweden with low sun angle and often cloudy weather[76] and where much of the nonclear-cutting harvest activities took place in small and irregular areas[77], *GFW* tree cover data likely had a lower f_{loss} compared with regional data from the Copernicus Land Monitoring Service[78,79] (**Figs. S25 a-c**). In contrast, in the boreal region of Canada with widespread low-density tree communities[80] and significant wildfire losses in less productive forests that require long recovery times[81], *GFW* tree cover data likely underestimated f_{gain} compared with data from the National Terrestrial Ecosystem Monitoring System[65] (**Fig. S26 a-c**). Results based on these regional datasets indicated a weaker positive asymmetry of f_{gain} on *LST* neutrality in northern Europe ($\Delta\rho$=-0.12 ±0.010) but a stronger one in Canada ($\Delta\rho$=0.07±0.023) (plots d-i in **Fig. S25-26**).

Overall, the asymmetric patterns of ΔLST_{fc} with respect to the newly calibrated f_{gain} versus f_{loss} from regional tree cover datasets are consistent with those of *GFW*.

Uncertainties caused by the asymmetric patterns of ΔLST_{fc} in the time-series analysis and space-for-time analogy

Repeated and consistent satellite observations have been widely used to quantify the direct biophysical effects of forest cover changes on *LST* from a global perspective[5,22,24,41,44]. The most difficult challenge in the time-series analysis has been how to separate direct biophysical effects of tree cover changes from climate variability[5,36]. To overcome this challenge, Alkama and Cescatti[5] selected forest grid cells that experienced net-zero changes in forest cover and attributed their *LST* anomalies to climate variability. However, herein we highlighted an asymmetric effect of tree cover gain versus loss on *LST* induced by their direct biophysical processes so that forest grid cells with net-zero change in forest cover may lead to either a negative or positive *LST* anomaly, depending highly on the background climate and magnitude of gross tree cover gain and loss with distinct biophysical properties. Therefore, an optimal reference in the time-series analysis should be selected from undisturbed forests with no gross tree cover gain and loss to disentangle direct biophysical *LST* effects of forest cover changes from climate variability.

The space-for-time analogy is a common approach for estimating the direct biophysical effects of forest cover changes on *LST*[13,24]. However, inconsistencies in both sign and magnitude have been observed between satellite- and ground-based studies[24,42]. It has been argued that the ground-based, near-surface air temperature[7,12,23,82,83] was less sensitive to aerodynamic resistance[5,42,44] associated with forest cover changes than the satellite-based *LST* (i.e., skin temperature)[5,12,13,24,84], leading to the above controversies between satellite- and ground-based studies. The asymmetric patterns of ΔLST_{fc} in response to tree cover gain and loss can provide an alternative explanation. Satellite-based *LST* from coarse and moderate sensors usually sample a land pixel which represents the mixed biophysical *LST* effects of sub-grid gross tree cover gains and losses. In contrast, tower studies have a smaller footprint and sample small forest stands[50,85,86]. However, this mismatch in spatial scales was mostly neglected in space-for-time methods to infer the biophysical effects of forest cover change, as this approach simplifies that the temperature differences between paired sites are explained solely by net differences in forest cover[42].

Limitations and potential implications

The most significant limitation is the accuracy and consistency of satellite signals in capturing fine-scale tree cover changes globally. While many satellite tree cover data are regionally validated, it is important to recognize that a comprehensive validation using field inventory tree cover data remains challenging[63], and in most cases is only partially implemented[64]. One important discrepancy between satellite-based and field inventory tree cover data is likely driven by forest management activities (e.g., harvest activity and selective thinning) which results in changes in tree cover, but not land cover change[71]. Thus, global tree cover datasets fully validated by field inventory tree cover data are necessary for accurately quantifying the direct biophysical effects of global forests in the future.

Second, planting or regenerating trees in previously disturbed forests to restore their biophysical cooling are one of the important natural climate solutions to mitigate local surface warming[46]. Nevertheless, the direct biophysical temperature effect analyzed in this study is different from the full climate impacts, involving both indirect biophysical[87,88] and biogeochemical effects[89,90]. Indirect biophysical effects tend to enhance clouds over temperate and boreal forests but inhibit cloud formation over tropical/subtropical forests[14]. Thus, ongoing fine-scale tree cover changes could either dampen or amplify surface temperature change through their indirect biophysical[88,91-94] and biogeochemical effects[95]. There is still a long way to go towards fully accounting for biogeochemical and direct/indirect biophysical changes[11,21,30,96,97] of fine-scale forest management in climate mitigation policies like the Paris Agreement[5,30,98].

In conclusion, our analysis provides a first global estimate of direct biophysical effects of gross tree cover gain and loss at fine resolution. It demonstrates an asymmetric effect of tree cover gain versus loss on *LST*. This result helps quantifying an average ratio of tree cover gain to loss to achieve a net direct biophysical cooling, which could be considered for climate-smart forest management[99]. Moreover, the asymmetric patterns of direct biophysical effects on *LST* may also result in various cascading effects on biodiversity (e.g., species distribution)[100], functional traits (e.g., leaf phenology)[101,102], and ecosystem functioning (e.g., photosynthesis)[103], which are strongly driven by local temperatures[100].

Methods

Calculating fractions of gross tree cover gains and losses

As an initial step, we overlaid the 30-m high-resolution global tree cover change maps from Global Forest Watch (*GFW*)[15] onto 0.05° resolution MODIS MCD12C1 land cover images[39], and selected the grid cells that were defined as "forestlands" in the MODIS land cover images. The 0.05° resolution forest grid cells that had experienced fractional gains (f_{gain}>0.02) or losses (f_{loss}>0.02) in tree cover from 2000 to 2012 based on *GFW* tree cover maps were considered as disturbed forests (stand-replacing natural disturbance, forest management, changes in canopy density etc.). The f_{gain} and f_{loss} denote the fractions of tree cover gain and tree cover loss for the 0.05° grid cell, respectively.

GFW maps recorded three types of pixels, i.e., tree cover gain, loss, and both[15], while only had the tree cover fraction information for 30-m resolution pixels in 2000. Here, we estimated the fractions of tree cover gain and loss for the 0.05° disturbed forest grid cell in 2012 by taking 2000 as the benchmark year. Overall, three cases were considered: (i) In a 0.05° resolution forest grid cell *k*, for pixel *i* labelled only "forest loss" in *GFW* 30-m resolution maps, the tree cover decreased from the fraction (f_i^{30m}) in 2000 to zero by 2012; this is a direct estimate of f_{loss} using *GFW* tree cover data. (ii) For pixel *j* labelled only "forest gain", we assumed that the tree cover would increase to the average values ($f_{ref,j}^{30m}$) of neighboring well-grown forests (surrounding 9×9 pixels) with tree cover fractions higher than 50%. To verify this assumption, we compared the tree cover fraction of a forest planted from 1982 to 2000[50] to the tree cover fractions of well-grown forests (9×9 pixels) surrounding that planted forest. The results show that the fractions were strongly and linearly correlated along the 1:1 diagonal line (all R^2 values >0.98, **Fig. S27**). (iii) For pixel *z* with both tree cover gains and losses, we assumed that the tree cover would initially decrease from the fraction (f_z^{30m}) in 2000 to zero, as did the pixels labelled only "forest loss". Then, we assumed that the tree cover fractions would increase to the average fraction ($f_{ref,z}^{30m}$) of surrounding well-grown forests in 2012, similar to pixels labelled only "forest gain". Thus, the average fraction of tree cover losses ($f_{loss,k}^{0.05°}$) and gains ($f_{gain,k}^{0.05°}$) for disturbed forest grid cell *k* was calculated using **Equations 1** and **2**, respectively.

$$f_{loss,k}^{0.05°} = \left[\sum_1^i (f_i^{30m}) + \sum_1^z (f_z^{30m})\right] \times \frac{0.00025 \times 0.00025}{0.05 \times 0.05} \quad (1)$$

$$f_{gain,k}^{0.05°} = \left[\sum_1^j \left(f_{ref,j}^{30m} - f_j^{30m}\right) + \sum_1^z \left(f_{ref,z}^{30m}\right)\right] \times \frac{0.00025 \times 0.00025}{0.05 \times 0.05} \quad (2)$$

where $f_{gain,k}^{0.05°}$ and $f_{loss,k}^{0.05°}$ denote the fractions of tree cover gains and tree cover losses for the 0.05°disturbed forest grid cell k, respectively. f_i^{30m} represents the tree cover fraction of the 30-m (~0.0025°) resolution grid *i* within the 0.05° forest grid k in 2000. f_{ref}^{30m} represents the average tree cover fraction of surrounding 9×9 30-m resolution pixels with tree cover fractions higher than 50% around the target pixel in 2000. *i* and *j* denote the number of 30-m resolution pixels labelled as only forest gains and losses, respectively. *z* denotes the number of 30-m resolution pixels that experienced both forest gains and losses. $\frac{0.00025 \times 0.00025}{0.05 \times 0.05}$ is the conversion coefficient, which is the ratio of the spatial resolution in *GFW* tree cover maps to that of the MODIS MCD12C1 land cover maps. We then selected the 0.05° grid cells with tree cover gain (f_{gain}>0.02) or loss fractions (f_{loss}>0.02) during the study period (2000-2012) in *GFW* tree cover change datasets as the disturbed forest grid cell for the analyses.

Calculating ΔLST_{fc} caused by tree cover gains and losses

We used the 0.05° resolution MOD11C3 v061 daytime and nighttime LST products[38] (refers to the skin temperature of land surfaces[5,7,38,42]) to represent the daytime and nighttime *LST*, respectively, and calculated the daily mean LST by averaging the MODIS daytime and nighttime LST. As the temperature anomaly (ΔLST_{total}) between two years in a given disturbed forest grid cell was the combined effect induced by both tree cover change and climate variability[5], we used the time-series analysis methodology developed by Alkama and Cescatti[5] (**Equation 3**) to disentangle the direct biophysical effect of tree fractional gain and loss (ΔLST_{fc}) from that due to climate variability (ΔLST_{cv}).

In the method by Alkama and Cescatti[5], forest grid cells with f_{net}=0±0.02 were defined as reference undisturbed forests for estimating ΔLST_{cv}. In our methods, instead, more stringent criteria were used to constrain the undisturbed grid cells: (1) to eliminate impacts from tree cover changes, both f_{gain} and f_{loss} in undisturbed forest grid cells should be smaller than 0.02 over 2000-2012; and (2) to eliminate impacts from forest degradation, undisturbed grid cells should also have small variations in the Normalized Difference Vegetation Index (NDVI) ($\Delta NDVI$=0±0.02) during the same period. For a certain disturbed forest grid cell, its reference grid cells were detected from neighboring undisturbed forests located within a distance of 50km[5], as grid cells within 50 km were assumed to share the most similar climate background[24]. We then took the temperature anomalies of reference undisturbed grid cells between 2000 and 2012 as those induced by climate variability without the interference of tree cover changes (i.e., $\Delta LST_{fc} \approx 0$ and $\Delta LST_{total} = \Delta LST_{cv}$). To limit the influence caused by distance, all ΔLST_{cv} values within 50 km of the disturbed forest grid cells were averaged using the inverse distance as a weighting factor, as shown in **Equation 4**[5],

$$\Delta LST_{fc} = \Delta LST_{total} - \Delta LST_{cv} \tag{3}$$

$$\Delta LST_{cv} = \frac{\sum_{k=1}^{n} \frac{\Delta LST_k}{d_k}}{\sum_{k=1}^{n} \frac{1}{d_k}} \tag{4}$$

where ΔLST_{total} (°C) signifies the overall LST change in disturbed forest grid cells; ΔLST_{fc} (°C) denotes the LST change in disturbed forest grid cells caused by tree cover gains and losses; ΔLST_{cv} (°C) is the LST change induced by climate variability; ΔLST_k (°C) denotes the LST changes in reference undisturbed forest grid cells (k) and d_k is the distance between the disturbed and undisturbed forest grid cells (k) in km.

We further quantified the sensitivity of ΔLST_{fc} to the fraction of tree cover gain (f_{gain}) and tree cover loss (f_{loss}) with a linear regression model as follows:

$$\Delta LST_{fc} = S_{gain} \times f_{gain} + S_{loss} \times f_{loss} \tag{5}$$

where S_{gain} (°C) and S_{loss} (°C) express the sensitivities of ΔLST_{fc} to f_{gain} and f_{loss}, respectively. Here, grid cells were analyzed using a moving window of 6×6°, shifted by 2° at each step, as shown in **Fig. 1c, d**.

Detecting asymmetric patterns of ΔLST_{fc} and temperature-neutral curves induced by tree cover gains versus losses

Bubble matrix plots were used to show asymmetric responses of ΔLST_{fc} with respect to f_{gain} versus f_{loss}. As shown in **Fig. S28,** in the bubble matrix, the colour of each cell represents the average value of ΔLST_{fc} observed for a given combination of f_{gain} and f_{loss} within the 0.05° grid cell. Red denotes a warming effect (ΔLST_{fc}>0.02°C), blue indicates cooling (ΔLST_{fc}<-0.02°C) and grey represents a net-zero temperature change (ΔLST_{fc}=0.0±0.02°C) between 2000 and 2012. The X- and Y- axes representing the f_{loss} and f_{gain}, respectively, were plotted schematically in the 0.2 bin in **Fig. S28** and the 0.02 bin in **Fig. 2**.

The *LST*-neutral curve was defined as the boundary between dots with negative ΔLST_{fc} (cooling) and dots with positive ΔLST_{fc} (warming) in the [f_{gain}, f_{loss}] space. To simulate the *LST*-neutral curve, we selected the dots with ΔLST_{fc}=0.0±0.02°C in the bubble matrix plots (**Fig. 2**). We then examined multiple linear and nonlinear (e.g., quadratic, cubic, general additive models) regressions to fit the relationships between f_{gain} and f_{loss} and used the Akaike Information Criterion (AIC) to select the optimal model[104]. Finally, a quadratic function was chosen as the best model to regress the nonlinear relationship between f_{gain} and f_{loss} where ΔLST_{fc}= 0.0±0.02°C: $f_{gain} = q(f_{loss})$, as depicted by the black solid curves in **Fig. 2**.

Assessing the surface energy balance to interpret the asymmetric patterns of ΔLST_{fc}

Net solar radiation received on the ground is converted into sensible heat flux (*H*), latent heat flux (*LE*), and ground heat flux(*G*). The function of the surface energy balance is expressed as follows[13]:

$$SW_{\downarrow} - SW_{\uparrow} + LW_{\downarrow} - LW_{\uparrow} = LE + H + G \quad (6)$$

where $SW_{\downarrow}$ and $SW_{\uparrow}$ denote the downwelling shortwave radiative flux incidenting on the ground (total solar radiation) and reflected solar shortwave radiation from the surface (reflected shortwave radiation), respectively. $LW_{\downarrow}$ and $LW_{\uparrow}$ denote the longwave radiation from the atmosphere (atmospheric downward radiation) and longwave radiation emitted from the surface to the atmosphere (surface emitted radiation), respectively. LE is the latent heat flux referring to the transfer of heat due to the transitional phase of water in the atmosphere. H is the sensible heat flux referring to the heat transfer between the ground and air caused by the turbulent movement of the surface layer. G is the ground heat flux representing the quantity of energy transfer between the surface and deep soil.

Herein, we used the method of Duveiller and colleagues[13] to assess the potential impact of tree cover changes on the surface energy balance, which assumed that the tree cover change at 30-m resolution is not strong enough to induce cloud feedback and the assigned net-zero change in $SW_{\downarrow}$ and $LW_{\downarrow}$ (i.e., $\Delta SW_{\downarrow} = 0$ and $\Delta LW_{\downarrow} = 0$)[105]. The change in residual fluxes, composed of both H and G, can be estimated by **Equation 7**. Steps for the derivation of **Equation 7** are shown in the Supplementary Information.

$$\Delta(H + G)_{fc} = -\Delta SW_{\uparrow,fc} - \Delta LW_{\uparrow,fc} - \Delta LE_{fc} \tag{7}$$

where Δ refers to the changes in the components of the surface energy balance; the subscript fc represents changes in energy fluxes induced by tree cover changes; ΔLE_{fc} was calculated by removing the average ΔLE of reference undisturbed grid cells from that of corresponding disturbed forest grid cells.

The changes in the reflected shortwave radiation ($\Delta SW_{\uparrow,fc}$) in response to tree cover changes can be expressed as the product of changes in albedo ($\Delta albedo$) and shortwave downwelling radiative fluxes ($SW_{\downarrow}$), shown in **Equation 8**.

$$\Delta SW_{\uparrow,fc} = \Delta albedo \times SW_{\downarrow} \tag{8}$$

The changes in $LW_{\uparrow,fc}$ (referred to as $\Delta LW_{\uparrow,fc}$) in response to tree cover change can be physically derived using **Equation 9**[23]:

$$\Delta LW_{\uparrow,fc} = \epsilon \Delta LST_{fc} 4\sigma LST^{3} \tag{9}$$

where ϵ is broadband emissivity and σ represents the Stefan-Boltzmann constant (σ=5.67×10^{-8} W/(m^2·K^4)). MOD11C3 products[38] provide emissivity estimates, where ϵ can be calculated using an empirical equation[106]: $\epsilon = 0.2122\epsilon_{29} + 0.3859\epsilon_{31} + 0.4029\epsilon_{32}$. ϵ_{29}, ϵ_{31}, and ϵ_{32} represent the estimated emissivity in MODIS bands 29 (8400-8700 nm), 31 (10780-11280 nm) and 32 (11770-12270 nm).

The data sources of the components in surface energy balance are shown in **Table**

S1. The LE data for calculating ΔLE were derived from the MOD16A3GF v061 products[58]. The $albedo$ and $SW_{\downarrow}$ data for calculating $\Delta SW_{\uparrow,fc}$ were obtained from MCD43C3 v061 products at a 0.05° resolution and from GLASS DSR (V60) data at a 0.05° resolution[59], respectively. The daytime and nighttime LST data were from the MOD11C3 v061 LST products[38], while the daily mean ΔLST_{fc} for estimating $\Delta LW_{\uparrow,fc}$ was calculated as the average of the daytime and nighttime ΔLST_{fc}. The $\Delta(H+G)_{fc}$ component was calculated from $\Delta SW_{\uparrow,fc}$, $\Delta LW_{\uparrow,fc}$ and ΔLE_{fc} based on **Equation 7**.

Evaluating the influences of scale transformation, study period, tree age, disturbance driver and tree cover data on the asymmetric responses of ΔLST_{fc}

To assess potential uncertainties caused by scale transformation[107] that might be induced by matching 30-m resolution tree cover changes[15] with the 0.05° resolution MODIS land cover and LST data[39], we produced additional bubble matrix plots of ΔLST_{fc} at 0.1° resolution (**Fig. S6**) to compare with those at 0.05° resolution (**Fig. 2**). If the LST-neutral curves at the 0.1° and 0.05° resolutions varied significantly, the asymmetric patterns of ΔLST_{fc} were treated as strongly scale-dependent transformation, or otherwise were considered scale-independent or rarely scale-dependent. To assess potential uncertainties from our assumptions on f_{gain} in *GFW* tree cover data, we additionally plotted the asymmetric patterns of ΔLST_{fc} against f_{gain} versus f_{loss} under different scenarios for pixels with tree cover gain, whose final tree covers in 2012 were assumed to be 50% (minimum), 75% (moderate) and 100% (maximum), respectively (**Figs. S3-5**).

On *GFW* maps, the pixels of tree cover loss were recorded separately in each year from 2000 to 2012, while the pixels of tree cover gain were only given for the whole period without planting year information[15]. To allocate the fractions of tree cover gains to each year from 2000 to 2012, we overlaid *GFW* tree cover change map onto a 30-m resolution global dataset of tree plantations[50]. We subsequently assigned the information of planting years to corresponding 30-m resolution pixels labelled as tree cover gain on *GFW* maps. Considering the inconsistency in coverage between *GFW* tree cover maps and the tree plantation maps[50], only the 0.05° resolution grid cells, with more than 80% of total 30-m resolution pixels being assigned with planting year information, were included in the analysis. After allocating the fractions of tree cover gain yearly, we examined the asymmetric responses of ΔLST_{fc} and corresponding neutral curves for various combinations of f_{gain} and f_{loss} among the different time periods (i.e., 2003-2012, 2006-2012 and 2009-2012) (**Fig. S2**).

Next, by matching tree age information[50] with *GFW* tree cover maps, we quantified the influences of tree age on the asymmetric patterns of ΔLST_{fc} and corresponding *LST*-neutral curves for pixels at 0.05° resolution with different tree planting ages (i.e., ages ≤6 years versus 6 years<ages≤12 years) (**Figs. S15 and S16**). Additionally, we further used the space-for-time method over a longer period to quantify the impact of tree age on ΔLST_{fc} (**Fig. 5**). By matching the global tree plantation data of Du et al.[50] with the MODIS *LST* time-series, we estimated the ΔLST_{fc} by using the *LST* of forest grid cells minus the *LST* of reference nonforest grid cells within a 50-km radius of the forest grid cell[5]. Only the 0.05° resolution forest grid cells with more than 80% of their sub-grid 30-m resolution forest pixels assigned with information of planting trees based on Du's map were included in the analysis. To eliminate the influences of tree cover, forest grid cells with $50\% < f_{gain} \leq 70\%$ (**Fig. S17a, c, e**) and $f_{gain} > 70\%$ (**Fig. S17b, d, f**)) were analyzed separately.

Curtis et al.[40] classified five main drivers of tree cover loss in global forests (10-km resolution): commodity-driven deforestation (permanent conversion from forestland to nonforest land); forestry (large-scale forestry operations within forests), shifting agriculture (conversion from forest to agriculture lands), wildfire (burning of forest vegetation), and urbanization (conversion from forest to urban areas). To investigate the underlying mechanism, we graphed the bubble matrix plots of ΔLST_{fc} and changes in energy fluxes against f_{gain} and f_{loss} for disturbed forest grid cells with different drivers of tree cover loss, respectively (**Figs. S9-14**).

Finally, we used five regional forest cover datasets in Canada[65], USA[66], eastern Europe[67], northern Europe[68], China[69], and the whole tropical region[70] (**Table S2**) to test potential uncertainties from tree cover change data. For regional tree cover data, we classified the 30-m resolution pixels of forest gain and loss as follows: (1) forest pixels converted from other land cover types are recognized as type of "forest gain"; (2) nonforest pixels converted from forests are detected as type of "forest loss"; (3) pixels having ever undergone both processes (1) and (2) are recognized as type of "forest gain and loss". Then, we compared f_{gain} and f_{loss} in *GFW* tree cover data with those of the newly generated tree cover datasets, calibrated by national forest cover statistics or field forest inventory data (**Fig. S20**), at 0.05° resolution and tested the asymmetric patterns of ΔLST_{fc} in response to f_{gain} versus f_{loss} (**Figs. S21-26**).

Acknowledgments

We sincerely thank the editor and anonymous reviewers for their insightful comments and valuable suggestions. We also thank Dr. Nicholas Coops from The University of British Columbia and Dr. Sergey Bartalev from Russian Academy of Sciences for providing the regional tree cover datasets and editing the paper. This study was supported by the National Natural Science Foundation of China (Nos. 41971275, 31971458, and U21A6001), the Guangdong Major Project of Basic and Applied Basic Research (No. 2020B0301030004), and Innovation Group Project of Southern Marine Science and Engineering Guangdong Laboratory (Zhuhai) (No. 311021009).

Data Availability

The land surface temperature, land cover, evapotranspiration, albedo, forest age, and energy flux data used for the analyses in this study are available online as follows, 30-m resolution *GFW* maps of 21st-century forest cover change: https://glad.earthengine.app/view/global-forest-change; MOD11C3 LST product: https://lpdaac.usgs.gov/products/mod11c3v061/; MCD12C1 Land Cover dataset: https://lpdaac.usgs.gov/products/mcd12c1v061/; MCD43C3 Albedo product: https://lpdaac.usgs.gov/products/mcd43c3v061/; MOD16A2GF ET and LE product: https://lpdaac.usgs.gov/products/mod16a2v061/; GLASS Shortwave Radiation product: http://www.glass.umd.edu/Download.html; MOD13C2 NDVI product: https://lpdaac.usgs.gov/products/mod13c2v061/; drivers of global forest loss:

https://www.science.org/doi/abs/10.1126/science.aau3445; GLASS ET product: http://www.glass.umd.edu/Download.html; PML_V2 ET product: https://data.tpdc.ac.cn/zh-hans/data/48c16a8d-d307-4973-abab-972e9449627c/; the latest digital Köppen-Geiger world map: http://koeppen-geiger.vu-wien.ac.at/present.htm; global map of planting years: https://figshare.com/articles/dataset/A_global_map_of_planting_years_of_plantations/19070084/1; forest cover change data of Canada: https://opendata.nfis.org/mapserver/nfis-change_eng.html; forest cover change data of northern Europe: https://land.copernicus.eu/pan-european/high-resolution-layers/forests/tree-cover-density/change-maps; forest cover change data of eastern Europe: https://glad.geog.umd.edu/dataset/eastern-europe-forset-cover-dynamics-1985-2012/; forest cover change data of the USA: https://www.mrlc.gov/data; and forest cover change data of the whole tropical region: https://forobs.jrc.ec.europa.eu/TMF/.

Code Availability

No custom code was developed for this study. All equations were given in Methods. The Origin (version 2022b) and ArcGIS (version 10.4) programs were used to generate all results.

Conflict of Interests

The authors declare no competing interests.

References

1. Carvalhais, N., Forkel, M., Khomik, M., Bellarby, J., Jung, M., Migliavacca, M., Mu, M., Saatchi, S., Santoro, M., Thurner, M., Weber, U., Ahrens, B., Beer, C., Cescatti, A., Randerson, J. T. & Reichstein, M. Global covariation of carbon turnover times with climate in terrestrial ecosystems. Nature 514, 213-217 (2014).
2. Le Quéré, C., Peters, G. P., Andres, R. J., Andrew, R. M., Boden, T. A., Ciais, P., Friedlingstein, P., Houghton, R. A., Marland, G., Moriarty, R., Sitch, S., Tans, P.,

Arneth, A., Arvanitis, A., Bakker, D. C. E., Bopp, L., Canadell, J. G., Chini, L. P., Doney, S. C., Harper, A., Harris, I., House, J. I., Jain, A. K., Jones, S. D., Kato, E., Keeling, R. F., Klein Goldewijk, K., Körtzinger, A., Koven, C., Lefèvre, N., Maignan, F., Omar, A., Ono, T., Park, G. - H., Pfeil, B., Poulter, B., Raupach, M. R., Regnier, P., Rödenbeck, C., Saito, S., Schwinger, J., Segschneider, J., Stocker, B. D., Takahashi, T., Tilbrook, B., van Heuven, S., Viovy, N., Wanninkhof, R., Wiltshire, A. & Zaehle, S. Global carbon budget 2013. Earth Syst. Sci. Data 6, 235-263 (2014).

3. Friedlingstein, P., Jones, M. W., O'Sullivan, M., Andrew, R. M., Hauck, J., Peters, G. P., Peters, W., Pongratz, J., Sitch, S., Le Quéré, C., Bakker, D. C. E., Canadell, J. G., Ciais, P., Jackson, R. B., Anthoni, P., Barbero, L., Bastos, A., Bastrikov, V., Becker, M., Bopp, L., Buitenhuis, E., Chandra, N., Chevallier, F., Chini, L. P., Currie, K. I., Feely, R. A., Gehlen, M., Gilfillan, D., Gkritzalis, T., Goll, D. S., Gruber, N., Gutekunst, S., Harris, I., Haverd, V., Houghton, R. A., Hurtt, G., Ilyina, T., Jain, A. K., Joetzjer, E., Kaplan, J. O., Kato, E., Klein Goldewijk, K., Korsbakken, J. I., Landschützer, P., Lauvset, S. K., Lefèvre, N., Lenton, A., Lienert, S., Lombardozzi, D., Marland, G., McGuire, P. C., Melton, J. R., Metzl, N., Munro, D. R., Nabel, J. E. M. S., Nakaoka, S.-I., Neill, C., Omar, A. M., Ono, T., Peregon, A., Pierrot, D., Poulter, B., Rehder, G., Resplandy, L., Robertson, E., Rödenbeck, C., Séférian, R., Schwinger, J., Smith, N., Tans, P. P., Tian, H., Tilbrook, B., Tubiello, F. N., van der Werf, G. R., Wiltshire, A. J. & Zaehle, S. Global carbon budget 2019, Earth Syst. Sci. Data 11, 1783–1838 (2019).
4. Bonan, G. B. Forests and climate change: forcings, feedbacks, and the climate benefits of forests. Science 320, 1444-1449 (2008).
5. Alkama, R. & Cescatti, A. Biophysical climate impacts of recent changes in global forest cover. Science 351, 600-604 (2016).
6. Betts, R. A. Offset of the potential carbon sink from boreal forestation by decreases in surface albedo. Nature 408, 187-190 (2000).
7. Lee, X., Goulden, M. L., Hollinger, D. Y., Barr, A., Black, T. A., Bohrer, G., Bracho, R., Drake, B., Goldstein, A., Gu, L., Katul, G., Kolb, T., Law, B. E., Margolis, H.,

Meyers, T., Monson, R., Munger, W., Oren, R., Paw U, K. T., Richardson, A. D., Schmid, H. P., Staebler, R., Wofsy, S. & Zhao, L. Observed increase in local cooling effect of deforestation at higher latitudes. Nature 479, 384-387 (2011).

8. Mahmood, R., Pielke Sr, R. A., Hubbard, K. G., Niyogi, D., Dirmeyer, P. A., McAlpine, C., Carleton, A. M., Hale, R., Gameda, S., Beltrán-Przekurat, A., Baker, B., McNider, R., Legates, D. R., Shepherd, M., Du, J., Blanken, P. D., Frauenfeld, O. W., Nair, U. S. & Fall, S. Land cover changes and their biogeophysical effects on climate. Int. J. Climatol. 34, 929-953 (2014).
9. Zeng, Z., Piao, S., Li, L. Z. X., Zhou, L., Ciais, P., Wang, T., Li, Y., Lian, X., Wood, E. F., Friedlingstein, P., Mao, J., Estes, L. D., Myneni, R. B., Peng, S., Shi, X., Seneviratne, S. I. & Wang, Y. Climate mitigation from vegetation biophysical feedbacks during the past three decades. Nat. Clim. Change 7, 432-436 (2017).
10. Davin, E. L., de Noblet-Ducoudré, N. & Friedlingstein, P. Impact of land cover change on surface climate: relevance of the radiative forcing concept. Geophys. Res. Lett. 34 (2007).
11. Windisch, M. G., Davin, E. L. & Seneviratne, S. I. Prioritizing forestation based on biogeochemical and local biogeophysical impacts. Nat. Clim. Change 11, 867–871 (2021).
12. Bright, R. M, Davin, E., O'Halloran, T., Pongratz, J., Zhao, K. & Cescatti, A. Local temperature response to land cover and management change driven by non-radiative processes. Nat. Clim. Change 7, 296–302 (2017).
13. Duveiller, G., Hooker, J. & Cescatti, A. The mark of vegetation change on Earth's surface energy balance. Nat. Commun. 9, 679 (2018).
14. Xu, R., Li, Y., Teuling, A.J., Zhao, L., Spracklen, D.V., Garcia-Carreras, L., Meier, R., Chen, L., Zheng, Y., Lin, H. & Fu, B. Contrasting impacts of forests on cloud cover based on satellite observations. Nat. Commun. 13, 670 (2022).
15. Hansen, M. C., Potapov, P. V., Moore, R., Hancher, M., Turubanova, S. A., Tyukavina, A., Thau, D., Stehman, S. V., Goetz, S. J., Loveland, T. R., Kommareddy, A., Egorov, A., Chini, L., Justice, C. O. & Townshend, J. R. G. High-resolution global maps of 21st-century forest cover change. Science 342, 850-853 (2013).

16. Sterling, S., Ducharne, A. & Polcher, J. The impact of global land-cover change on the terrestrial water cycle. Nat. Clim. Change 3, 385–390 (2013).

17. Lejeune, Q., Davin, E. L., Gudmundsson, L., Winckler, J. & Seneviratne, S. I. Historical deforestation locally increased the intensity of hot days in northern mid-latitudes. Nat. Clim. Change 8, 386–390 (2018).

18. Liu, Z., Ballantyne, A. P. & Cooper, L. A. Biophysical feedback of global forest fires on surface temperature. Nat. Commun. 10, 214 (2019).

19. Claussen, M., Brovkin, V. & Ganopolski, A. Biogeophysical versus biogeochemical feedbacks of large-scale land cover change. Geophys. Res. Lett. 28, 1011-1014 (2001).

20. Wang, J., Ciais, P., Gasser, T., Chang, J., Tian, H., Zhao, Z., Zhu, L., Li, Z. & Li, W. Temperature Changes Induced by Biogeochemical and Biophysical Effects of Bioenergy Crop Cultivation. Environ. Sci. Technol. 57, 2474-2483 (2023).

21. Zhu, L., Li, W., Ciais, P., He, J., Cescatti, A., Santoro, M., Tanaka, K., Cartus, O., Zhao, Z., Xu, Y. & Sun, M. Comparable biophysical and biogeochemical feedbacks on warming from tropical moist forest degradation. Nat. Geosci. 1-6 (2023).

22. Peng, S. - S., Piao, S., Zeng, Z., Ciais, P., Zhou, L., Li, L. Z. X., Myneni, R. B., Yin, Y. & Zeng, H. Afforestation in China cools local land surface temperature. Proc. Natl Acad. Sci. 111, 2915-2919 (2014).

23. Luyssaert, S., Jammet, M., Stoy, P. C., Estel, S., Pongratz, J., Ceschia, E., Churkina, G., Don, A., Erb, K. H., Ferlicoq, M., Gielen, B., Grünwald, T., Houghton, R. A., Klumpp, K., Knohl, A., Kolb, T., Kuemmerle, T., Laurila, T., Lohila, A., Loustau, D., McGrath, M. J., Meyfroidt, P., Moors, E. J., Naudts, K., Novick, K., Otto, J., Pilegaard, K., Pio, C. A., Rambal, S., Rebmann, C., Ryder, J., Suyker, A. E., Varlagin, A., Wattenbach, M. & Dolman, A. J. Land management and land-cover change have impacts of similar magnitude on surface temperature. Nat. Clim. Change 4, 389-393 (2014)

24. Li, Y., Zhao, M., Motesharrei, S., Mu, Q., Kalnay, E. & Li, S. Local cooling and warming effects of forests based on satellite observations. Nat. Commun. 6, 6603 (2015).

25. Pickett, S.T. Space-for-time substitution as an alternative to long-term studies. Long-term studies in ecology: approaches and alternatives 110-135 (1989).

26. Senf, C. & Seidl, R. Mapping the forest disturbance regimes of Europe. Nat. Sustain. 4, 63-70 (2021).

27. Tong, X., Brandt, M., Yue, Y., Ciais, P., Jepsen, M. R., Penuelas, J., Wigneron, J. - P., Xiao, X., Song, X. - P., Horion, S., Rasmussen, K., Saatchi, S., Fan, L., Wang, K., Zhang, B., Chen, Z., Wang, Y., Li, X. & Fensholt, R. Forest management in southern China generates short term extensive carbon sequestration. Nat. Commun. 11, 1-10 (2020).

28. Heinrich, V.H., Dalagnol, R., Cassol, H.L., Rosan, T.M., de Almeida, C.T., Silva Junior, C.H., Campanharo, W.A., House, J.I., Sitch, S., Hales, T.C. & Adami, M. Large carbon sink potential of secondary forests in the Brazilian Amazon to mitigate climate change. Nat. Commun. 12, 1785 (2021).

29. Ryan, M. G., Binkley, D. & Fownes, J. H. Age-related decline in forest productivity: pattern and process. Adv. Ecol. Res. 27, 213–262 (1997).

30. Naudts, K., Chen, Y., McGrath, M. J., Ryder, J., Valade, A., Otto, J. & Luyssaert, S. Europe’s forest management did not mitigate climate warming. Science 351, 597-600 (2016).

31. Cooper, L. A., Ballantyne, A. P., Holden, Z. A. & Landguth, E. L. Disturbance impacts on land surface temperature and gross primary productivity in the western United States. J. Geophys. Res. Biogeosci. 122, 930-946 (2017).

32. Randerson, J. T., Liu, H., Flanner, M. G., Chambers, S. D., Jin, Y., Hess, P. G., Pfister, G., Mack, M. C., Treseder, K. K., Welp, L. R., Chapin, F. S., Harden, J. W., Goulden, M. L., Lyons, E., Neff, J. C., Schuur, E. A. G. & Zender, C. S. The impact of boreal forest fire on climate warming. Science 314, 1130-1132 (2006).

33. Maness, H., Kushner, P. J. & Fung, I. Summertime climate response to mountain pine beetle disturbance in British Columbia. Nat. Geosci. 6, 65-70 (2013).

34. O'Halloran, T. L., Law, B. E., Goulden, M. L., Wang, Z., Barr, J. G., Schaaf, C., Brown, M., Fuentes, J. D., Göckede, M., Black, A. & Engel, V. Radiative forcing of natural forest disturbances. Glob. Chang. Biol. 18, 555-565 (2012).

35. Rogers, B. M., Soja, A. J., Goulden, M. L. & Randerson, J. T. Influence of tree species on continental differences in boreal fires and climate feedbacks. Nat. Geosci. 8, 228-234 (2015).
36. Zeng, Z., Wang, D., Yang, L., Wu, J., Ziegler, A. D., Liu, M., Ciais, P., Searchinger, T. D., Yang, Z. - L., Chen, D., Chen, A., Li, L. Z. X., Piao, S., Taylor, D., Cai, X., Pan, M., Peng, L., Lin, P., Gower, D., Feng, Y., Zheng, C., Guan, K., Lian, X., Wang, T., Wang, L., Jeong, S. - J., Wei, Z., Sheffield, J., Caylor, K. & Wood, E. F. Deforestation-induced warming over tropical mountain regions regulated by elevation. Nat. Geosci. 14, 23-29 (2021).
37. Zhang, Y., & Liang, S. Impacts of land cover transitions on surface temperature in China based on satellite observations. Environ. Res. Lett. 13, 024010 (2018).
38. Wan, Z., Hook, S. & Hulley, G. MODIS/Terra Land Surface Temperature/Emissivity Monthly L3 Global 0.05Deg CMG V061 [Data set] (NASA EOSDIS Land Processes DAAC, 2021); https://doi.org/10.5067/MODIS/MOD11C3.061
39. Friedl, M. & Sulla-Menashe, D. MODIS/Terra+Aqua Land Cover Type Yearly L3 Global 0.05Deg CMG V061 [Data set] (NASA EOSDIS Land Processes DAAC, 2022); https://doi.org/10.5067/MODIS/MCD12C1.061.
40. Curtis, P. G., Slay, C. M., Harris, N. L., Tyukavina, A. & Hansen, M. C. Classifying drivers of global forest loss. Science 361, 1108-1111 (2018).
41. Su, Y., Liu, L., Wu, J., Chen, X., Shang, J., Ciais, P., Zhou, G., Lafortezza, R., Wang, Y., Yuan, W. Wang, Y., Zhang, H., Huang, G. & Huang, N. Quantifying the biophysical effects of forests on local air temperature using a novel three-layered land surface energy balance model. Environ. Int. 132, 105080 (2019).
42. Lawrence, D., Coe, M., Walker, W., Verchot, L. & Vandecar, K. The unseen effects of deforestation: Biophysical effects on climate. Front. For. Glob. Change 5, 756115 (2022).
43. Davin, E. L. & de Noblet-Ducoudré, N. Climatic impact of global-scale deforestation: radiative versus nonradiative processes. J. Clim. 23, 97–112 (2010).
44. Su, Y., Zhang, C., Chen, X., Liu, L., Ciais, P., Peng, J., Wu, S., Wu, J., Sheng, J.,

Wang, Y., Yuan, W., Yang, Y., Wu, Z. & Lafortezza, R. Aerodynamic resistance and Bowen ratio explain the biophysical effects of forest cover on understory air and soil temperatures at the global scale. Agric. Meteorol. 308, 108615 (2021).

45. Malhi, Y., Baldocchi, D. D. & Jarvis, P. G. The carbon balance of tropical, temperate and boreal forests. Plant Cell Environ. 22, 715-740 (1999).

46. Cook-Patton, S. C., Leavitt, S. M., Gibbs, D., Harris, N. L., Lister, K., Anderson-Teixeira, K. J., Briggs, R. D., Chazdon, R. L., Crowther, T. W., Ellis, P. W., Griscom, H. P., Herrmann, V., Holl, K. D., Houghton, R. A., Larrosa, C., Lomax, G., Lucas, R., Madsen, P., Malhi, Y., Paquette, A., Parker, J. D., Paul, K., Routh, D., Roxburgh, S., Saatchi, S., Hoogen, J. V. D., Walker, W. S., Wheeler, C. E., Wood, S. A., Xu, L. & Griscom, B. W. Mapping carbon accumulation potential from global natural forest regrowth. Nature 585, 545-550 (2020).

47. Moore, G. W., Bond, B. J., Jones, J. A., Phillips, N. & Meinzer, F. C. Structural and compositional controls on transpiration in the 40- and 450-year-old riparian forests in western Oregon, USA. Tree Physiol. 24, 481-491 (2004).

48. Jassal, R. S., Black, T. A., Spittlehouse, D. L., Brümmer, C. & Nesic, Z. Evapotranspiration and water use efficiency in different-aged Pacific Northwest Douglas-fir stands. Agric. Meteorol. 149, 1168-1178 (2009).

49. Stoy, P. C., Katul, G. G., Siqueira, M. B. S., Juang, J. Y., Novick, K. A., McCarthy, H. R., Christopher Oishi., A., Uebelherr, J. M., Kim, H. S. & Oren, R. Separating the effects of climate and vegetation on evapotranspiration along a successional chronosequence in the southeastern US. Glob. Chang. Biol. 12, 2115-2135 (2006).

50. Du, Z., Yu, L., Yang, J., Xu, Y., Chen, B., Peng, S., Zhang, T., Fu, H., Harris, N. & Gong, P. A global map of planting years of plantations. Sci. Data 9, 1-9 (2022).

51. Aryal, D. R., De Jong, B. H. J., Ochoa-Gaona, S., Esparza-Olguin, L. & Mendoza-Vega, J. Carbon stocks and changes in tropical secondary forests of southern Mexico. Agric. Ecosyst. Environ. 195, 220-230 (2014).

52. Potter, S., Solvik, K., Erb, A., Goetz, S. J., Johnstone, J. F., Mack, M. C., Randerson, J. T., Román, M. O., Schaaf, C. L., Turetsky, M. R., Veraverbeke, S., Walker, X. J., Wang, Z., Massey, R. & Rogers, B. M. Climate change decreases the cooling effect

from postfire albedo in boreal North America. Glob. Chang. Biol. 26, 1592-1607 (2020).

53. He, T., Liang, S. & Song, D. X. Analysis of global land surface albedo climatology and spatial-temporal variation during 1981–2010 from multiple satellite products. J. Geophys. Res. Atmos. 119, 281-298 (2014).

54. Gao, F., He, T., Wang, Z., Ghimire, B., Shuai, Y., Masek, J. G., Schaaf, C. & Williams, C. Multiscale climatological albedo look-up maps derived from MODIS BRDF/albedo products. J. Appl. Remote Sens. 8, 083532 (2014).

55. Baldocchi, D., Kelliher, F. M., Black, T. A. & Jarvis, P. Climate and vegetation controls on boreal zone energy exchange. Glob. Chang. Biol. 6, 69-83 (2000).

56. Oris, F., Asselin, H., Ali, A. A., Finsinger, W. & Bergeron, Y. Effect of increased fire activity on global warming in the boreal forest. Environ. Rev. 22, 206-219 (2014).

57. Anderson, R. G., Canadell, J. G., Randerson, J. T., Jackson, R. B., Hungate, B. A., Baldocchi, D. D., Ban-Weiss, G. A., Bonan, G. B., Caldeira, K., Cao, L., Diffenbaugh, N. S., Gurney, K. R., Kueppers, L. M., Law, B. E., Luyssaert, S. & O'Halloran, T. L. Biophysical considerations in forestry for climate protection. Front. Ecol. Environ. 9, 174–182 (2011).

58. Running, S., Mu, Q., Zhao, M. & Moreno, A. MODIS/Terra Net Evapotranspiration Gap-Filled Yearly L4 Global 500m SIN Grid V061 [Data set] (NASA EOSDIS Land Processes DAAC, 2021); https://doi.org/10.5067/MODIS/MOD16A3GF.061

59. Yao, Y. J., Liang, S., Cheng, J., Liu, S., Fisher, J. B., Zhang, X., Jia, K., Zhao, X., Qin, Q., Zhao, B., Han, S., Zhou, G., Zhou, G., Li, Y. & Zhao, S. MODIS-driven estimation of terrestrial latent heat flux in China based on a modified Priestley-Taylor algorithm. Agric. Meteorol. 171, 187-202 (2013).

60. Zhang, Y., Kong, D., Gan, R., Chiew, F. H. S., McVicar, T. R., Zhang, Q. & Yang, Y. Coupled estimation of 500m and 8-day resolution global evapotranspiration and gross primary production in 2002-2017. Remote Sens. Environ. 222, 165-182 (2019).

61. Tropek, R., Sedláček, O., Beck, J., Keil, P., Musilová, Z., Šímová, I. & Storch, D.

Comment on “High-resolution global maps of 21st-century forest cover change”. Science 344, 981-981 (2014).

62. Milodowski, D. T., Mitchard, E. T. A., & Williams, M. Forest loss maps from regional satellite monitoring systematically underestimate deforestation in two rapidly changing parts of the Amazon. Environ. Res. Lett. 12, 094003 (2017).

63. Breidenbach, J., Ellison, D., Petersson, H., Korhonen, K.T., Henttonen, H.M., Wallerman, J., Fridman, J., Gobakken, T., Astrup, R. & Næsset, E. Harvested area did not increase abruptly—how advancements in satellite-based mapping led to erroneous conclusions. Ann. For. Sci. 79, 1-9 (2022).

64. Ogle, S.M., Domke, G., Kurz, W.A., Rocha, M.T., Huffman, T., Swan, A., Smith, J.E., Woodall, C. & Krug, T. Delineating managed land for reporting national greenhouse gas emissions and removals to the United Nations framework convention on climate change. Carbon Balance Manag. 13, 1-13 (2018).

65. Hermosilla, T., Wulder, M.A., White, J.C., Coops, N.C., Hobart, G.W. & Campbell, L.B. Mass data processing of time series Landsat imagery: pixels to data products for forest monitoring. Int. J. Digit. Earth. 9(11), 1035-1054 (2016).

66. Dewitz, J. & USGS (US Geological Survey). National Land Cover Database (NLCD) 2019 Products; (Ver. 2.0, June 2021). US Geological Survey: Reston, Virginia, USA (2021).

67. Potapov, P.V., Turubanova, S.A., Tyukavina, A., Krylov, A.M., McCarty, J.L., Radeloff, V.C. & Hansen, M.C. Eastern Europe's forest cover dynamics from 1985 to 2012 quantified from the full Landsat archive. Remote Sens. Environ. 159, 28-43 (2015).

68. European Union, Copernicus Land Monitoring Service 2023, European Environment Agency (EEA).

69. Guo, J., Gong, P., Dronova, I. & Zhu, Z. Forest cover change in China from 2000 to 2016. Int. J. Remote Sens. 43, 593-606 (2022).

70. Vancutsem, C., Achard, F., Pekel, J.F., Vieilledent, G., Carboni, S., Simonetti, D., Gallego, J., Aragao, L.E. & Nasi, R. Long-term (1990-2019) monitoring of forest cover changes in the humid tropics. Sci. Adv. 7, eabe1603 (2021).

71. Barrett, F., McRoberts, R. E., Tomppo, E., Cienciala, E. & Waser, L. T. Remote Sensing of Environment A questionnaire-based review of the operational use of remotely sensed data by national forest inventories. Remote Sens. Environ. 174, 279-289 (2016).

72. McRoberts, R.E., Næsset, E., Liknes, G.C., Chen, Q., Walters, B.F., Saatchi, S. & Herold, M. Using a finer resolution biomass map to assess the accuracy of a regional, map-based estimate of forest biomass. Surv. Geophys. 40, 1001-1015 (2019).

73. Cunningham, D., Cunningham, P. & Fagan, M. E. Identifying biases in global tree cover products: a case study in Costa Rica. Forests 10, 853 (2019).

74. Sannier, C., McRoberts, R. E. & Fichet, L. V. Suitability of Global Forest Change data to report forest cover estimates at national level in Gabon. Remote Sens. Environ. 173, 326-338 (2016).

75. Hojas-Gascon, L., Cerutti, P. O., Eva, H., Nasi, R. & Martius, C. Monitoring Deforestation and Forest Degradation in the Context of REDD+: Lessons from Tanzania. Vol. 124 (CIFOR, 2015).

76. Pitkänen, T. P., Sirro, L., Häme, L., Häme, T., Törmä, M., & Kangas, A. Errors related to the automatized satellite-based change detection of boreal forests in Finland. Int. J. Appl. Earth. Obs. Geoinf. 86, 102011 (2020).

77. Jutras-Perreault, M.C., Gobakken, T. & Ørka, H.O. Comparison of two algorithms for estimating stand-level changes and change indicators in a boreal forest in Norway. Int. J. Appl. Earth. Obs. Geoinf. 98, 102316 (2021).

78. Palahí, M., Valbuena, R., Senf, C., Acil, N., Pugh, T.A., Sadler, J., Seidl, R., Potapov, P., Gardiner, B., Hetemäki, L. & Chirici, G. Concerns about reported harvests in European forests. Nature 592, E15-E17 (2021).

79. Chirici, G., Giannetti, F., Mazza, E., Francini, S., Travaglini, D., Pegna, R. & White, J.C. Monitoring clearcutting and subsequent rapid recovery in Mediterranean coppice forests with Landsat time series. Ann. For. Sci. 77, 1-14 (2020).

80. Timoney, K. P. & Mamet, S. No treeline advance over the last 50 years in subarctic western and central Canada and the problem of vegetation misclassification in remotely sensed data. Écoscience 27, 93-106 (2020).

81. Guindon, L., Bernier, P., Gauthier, S., Stinson, G., Villemaire, P., & Beaudoin, A. Missing forest cover gains in boreal forests explained. Ecosphere 9, e02094 (2018).
82. Vanden, B. S., Luyssaert, S., Davin, E. L., Janssens, I. & van Lipzig, N. New insights in the capability of climate models to simulate the impact of LUC based on temperature decomposition of paired site observations. J. Geophys. Res. Atmos. 120, 5417–5436 (2015).
83. Liao, W., Rigden, A. J. & Li, D. Attribution of local temperature response to deforestation. J. Geophys. Res. Biogeosci. 123, 1572–1587 (2018).
84. Prevedello, J. A., Winck, G. R., Weber, M. M., Nichols, E. & Sinervo, B. Impacts of forestation and deforestation on local temperature across the globe. PLoS One 14, e0213368 (2019).
85. George-Chacón, S. P., Mas, J. F., Dupuy, J. M., Castillo-Santiago, M. A. & Hernández-Stefanoni, J. L. Mapping the spatial distribution of stand age and aboveground biomass from Landsat time series analyses of forest cover loss in tropical dry forests. Remote Sens. Ecol. Conserv. 8, 347-361 (2022).
86. Schultz, N. M., Lawrence, P. J. & Lee, X. Global satellite data highlights the diurnal asymmetry of the surface temperature response to deforestation. J. Geophys. Res. Biogeosci. 122, 903–917 (2017).
87. Teuling, A.J., Taylor, C.M., Meirink, J.F., Melsen, L.A., Miralles, D.G., Van Heerwaarden, C.C., Vautard, R., Stegehuis, A.I., Nabuurs, G.J. & de Arellano, J.V.G. Observational evidence for cloud cover enhancement over western European forests. Nat. Commun. 8, 14065 (2017).
88. Duveiller, G., Filipponi, F., Ceglar, A., Bojanowski, J., Alkama, R., & Cescatti, A. Revealing the widespread potential of forests to increase low level cloud cover. Nat. Commun. 12, 4337 (2021).
89. Duveiller, G., Filipponi, F., Ceglar, A., Bojanowski, J., Alkama, R. & Cescatti, A. Biomass resilience of Neotropical secondary forests. Nature 530, 211–214 (2016).
90. Requena Suarez, D., Rozendaal, D.M., De Sy, V., Phillips, O.L., Alvarez-Dávila, E., Anderson-Teixeira, K., Araujo-Murakami, A., Arroyo, L., Baker, T.R., Bongers, F. & Brienen, R.J. Estimating aboveground net biomass change for tropical and

subtropical forests: refinement of IPCC default rates using forest plot data. Glob. Chang. Biol. 25, 3609–3624 (2019).

91. Leite-Filho, A. T., Soares-Filho, B. S., Davis, J. L., Abrahão, G. M. & Börner, J. Deforestation reduces rainfall and agricultural revenues in the Brazilian Amazon. Nat. Commun. 12, 2591 (2021).
92. Duku, C. & Hein, L. The impact of deforestation on rainfall in Africa: a data driven assessment. Environ. Res. Lett. 16, 064044 (2021).
93. Meier, R., Schwaab, J., Seneviratne, S. I., Sprenger, M., Lewis, E., & Davin, E. L. Empirical estimate of forestation-induced precipitation changes in Europe. Nat. Geosci. 14, 473–478 (2021).
94. Cerasoli, S., Yin, J. & Porporato, A. Cloud cooling effects of afforestation and reforestation at midlatitudes. Proc. Natl Acad. Sci. USA 118, e2026241118 (2021).
95. Seidl, R., Schelhaas, M. J., Rammer, W. & Verkerk, P. J. Increasing forest disturbances in Europe and their impact on carbon storage. Nat. Clim. Change 4, 806–810 (2014).
96. Pielke Sr, R.A., Marland, G., Betts, R.A., Chase, T.N., Eastman, J.L., Niles, J.O., Niyogi, D.D.S. & Running, S.W. The influence of land-use change and landscape dynamics on the climate system: relevance to climate-change policy beyond the radiative effect of greenhouse gases. Philos. Trans. A Math. Phys. Eng. Sci. 360, 1705-1719 (2002).
97. Pielke Sr, R.A., Pitman, A., Niyogi, D., Mahmood, R., McAlpine, C., Hossain, F., Goldewijk, K.K., Nair, U., Betts, R., Fall, S. & Reichstein, M. Land use/land cover changes and climate: modeling analysis and observational evidence. Wiley Interdiscip. Rev. Clim. Change. 2, 828-850 (2011).
98. I.P.C.C. Climate change 2014 synthesis report. IPCC: Geneva, Szwitzerland (2014).
99. Bowditch, E., Santopuoli, G., Binder, F., Del Rio, M., La Porta, N., Kluvankova, T., Lesinski, J., Motta, R., Pach, M., Panzacchi, P. & Pretzsch, H. What is Climate-Smart Forestry? A definition from a multinational collaborative process focused on mountain regions of Europe. Ecosyst Serv. 43, 101113 (2020).
100. Zellweger, F., de Frenne, P., Lenoir, J., Vangansbeke, P., Verheyen, K.,

Bernhardt-Römermann, M., Baeten, L., Hedl, R., Berki, I., Brunet, J., van Calster, H., Chudomelova, M., Decocq, G., Dirnböck, T., Durak, T., Heinken, T., Jaroszewicz, B., Kopecky, M., Máliš, F., Macek, M., Malicki, M., Naaf, T., Nagel, T. A., Ortmann-Ajkai, A., Petřík, P., Pielech, R., Reczyńska, K., Schmidt, W., Standovár, T., Świerkosz, K., Teleki, B., Vild, O., Wulf, M. & Coomes, D. Forest microclimate dynamics drive plant responses to warming. Science 368, 772-775 (2020).

101. Meinzer, F. C., Bond, B. J. & Karanian, J. A. Biophysical constraints on leaf expansion in a tall conifer. Tree Physiol. 28, 197-206 (2008).

102. Chen, C., Li, D., Li, Y., Piao, S., Wang, X., Huang, M., Gentine, P., Nemani, R. R. & Myneni, R. B. Biophysical impacts of Earth greening largely controlled by aerodynamic resistance. Sci. Adv. 6, eabb1981 (2020).

103. Smith, N. G., Lombardozzi, D., Tawfik, A., Bonan, G. & Dukes, J. S. Biophysical consequences of photosynthetic temperature acclimation for climate. J. Adv. Model. Earth. Sy. 9, 536-547 (2017).

104. Sakamoto, Y., Ishiguro, M. & Kitagawa, G. Akaike information criterion statistics. Dordrecht, The Netherlands: D. Reidel. 81, 26853 (1986).

105. Zhang, M., Lee, X., Yu, G., Han, S., Wang, H., Yan, J., Zhang, Y., Li, Y., Ohta, T., Hirano, T., Kim, J., Yoshifuji, N. & Wang, W. Response of surface air temperature to small-scale land clearing across latitudes. Environ. Res. Lett. 9, 034002 (2014).

106. Wang, K., Wan, Z., Wang, P., Sparrow, M., Liu, J., Zhou, X. & Haginoya, S. Estimation of surface long wave radiation and broadband emissivity using Moderate Resolution Imaging Spectroradiometer (MODIS) land surface temperature/emissivity products. J. Geophys. Res. Atmos. 110, D11109 (2005).

107. Chen, J. M. Spatial scaling of a remotely sensed surface parameter by contexture. Remote Sens. Environ. 69, 30-42 (1999).